Quantitative Proteomics Identifies Reduced NRF2 Activity and Mitochondrial Dysfunction in Atopic Dermatitis

*JID*Open

Michael Koch[1], Tobias Kockmann[2,7], Elke Rodriguez[3,7], Ulrike Wehkamp[3], Paul Hiebert[1], Maya Ben-Yehuda Greenwald[1], Dora Stölzl[3], Hans-Dietmar Beer[4], Erwin Tschachler[5], Stephan Weidinger[3,8], Sabine Werner[1,8] and Ulrich auf dem Keller[6,8]

Atopic dermatitis is the most common inflammatory skin disease and is characterized by a deficient epidermal barrier and cutaneous inflammation. Genetic studies suggest a key role of keratinocytes in atopic dermatitis pathogenesis, but the alterations in the proteome that occur in the full epidermis have not been defined. Using a pressure-cycling technology and data-independent acquisition approach, we performed quantitative proteomics of epidermis from healthy volunteers and lesional and nonlesional patient skin. Results were validated by targeted proteomics using parallel reaction monitoring mass spectrometry and immunofluorescence staining. Proteins that were differentially abundant in the epidermis of patients with atopic dermatitis versus in healthy control reflect the strong inflammation in lesional skin and the defect in keratinocyte differentiation and epidermal stratification that already characterizes nonlesional skin. Most importantly, they reveal impaired activation of the NRF2-antioxidant pathway and reduced abundance of mitochondrial proteins involved in key metabolic pathways in the affected epidermis. Analysis of primary human keratinocytes with small interfering RNA–mediated *NRF2* knockdown revealed that the impaired NRF2 activation and mitochondrial abnormalities are partially interlinked. These results provide insight into the molecular alterations in the epidermis of patients with atopic dermatitis and identify potential targets for pharmaceutical intervention.

INTRODUCTION

Atopic dermatitis (AD) affects at least 230 million people worldwide (Weidinger et al., 2018). It strongly reduces the QOL through recurrent eczematous skin lesions, itch, and frequent comorbidities such as asthma, allergic rhinitis, and food allergies. AD is driven by epidermal barrier defects and immunological alterations, promoting heightened type 2 responses and IgE-mediated sensitization to various allergens (Deckers et al., 2012; Weidinger et al., 2018). The impaired

[1]*Institute of Molecular Health Sciences, Department of Biology, ETH Zürich, Zürich, Switzerland;* [2]*Functional Genomics Center Zurich, University of Zurich/ETH Zürich, Zürich, Switzerland;* [3]*Department of Dermatology, Allergology and Venereology, University Hospital Schleswig-Holstein, Campus Kiel, Kiel, Germany;* [4]*Department of Dermatology, University Hospital Zurich, Zurich, Switzerland;* [5]*Research Division of Biology and Pathobiology of the Skin, Department of Dermatology, Medical University of Vienna, Vienna, Austria; and* [6]*Department of Biotechnology and Biomedicine, Technical University of Denmark, Lyngby, Denmark*

[7]*These authors contributed equally to this work.*

[8]*These authors contributed equally as senior authors.*

Correspondence: Ulrich auf dem Keller: Department of Biotechnology and Biomedicine, Technical University of Denmark, 2800 Kongens. Lyngby, Denmark. E-mail: uadk@dtu.dk

Abbreviations: AD, atopic dermatitis; Ctrl, control; K, keratin; KC, keratinocyte; MS, mass spectrometry; NL, nonlesional

A notice to readers: *The Editor of JID, Erwin Tschachler, who is an author on this publication, recused himself from the review of this submission. The article was externally peer reviewed according to JID's usual processes, and the decision to publish this article was made by a Deputy Editor.*

keratinocyte (KC) function might be causative, for example, because of inherited loss-of-function mutations in the gene encoding FLG (*FLG*), a structural protein with a crucial role in epidermal barrier function, or variations in other genes, such as genes encoding tight junction components (Brown et al., 2020; Weidinger et al., 2018). It can also be the consequence of the inflammatory milieu, as shown by the regulation of genes involved in KC differentiation by type 2 cytokines (Hönzke et al., 2016; Lou et al., 2017; Mitamura et al., 2018). Together, these features cause strong alterations in the gene expression program of different skin cell types, which are further promoted by pathogenic microorganisms and environmental factors. This has been supported by large-scale transcriptomic studies (Esaki et al., 2015; Guttman-Yassky et al., 2007; Nomura et al., 2003; Suárez-Fariñas et al., 2015; Tsoi et al., 2019). However, most of them used bulk skin tissue, and thus it was unclear whether the altered expression occurs in the epidermis and/or the dermis. Therefore, RNA profiling of epidermis and dermis isolated through laser capture microdissection or from samples of the upper epidermis obtained by tape stripping or single-cell RNA sequencing of total AD skin were performed, which revealed, for example, downregulation of different claudins in the epidermis and upregulation of various inflammatory markers (Esaki et al., 2015; Leung et al., 2019). To determine the AD proteome, isolated stratum corneum of adult patients with AD and control (Ctrl) individuals was used for mass spectrometry (MS)-based proteomics, which revealed a differential abundance of proteins involved in epidermal barrier function, inflammation, and antimicrobial
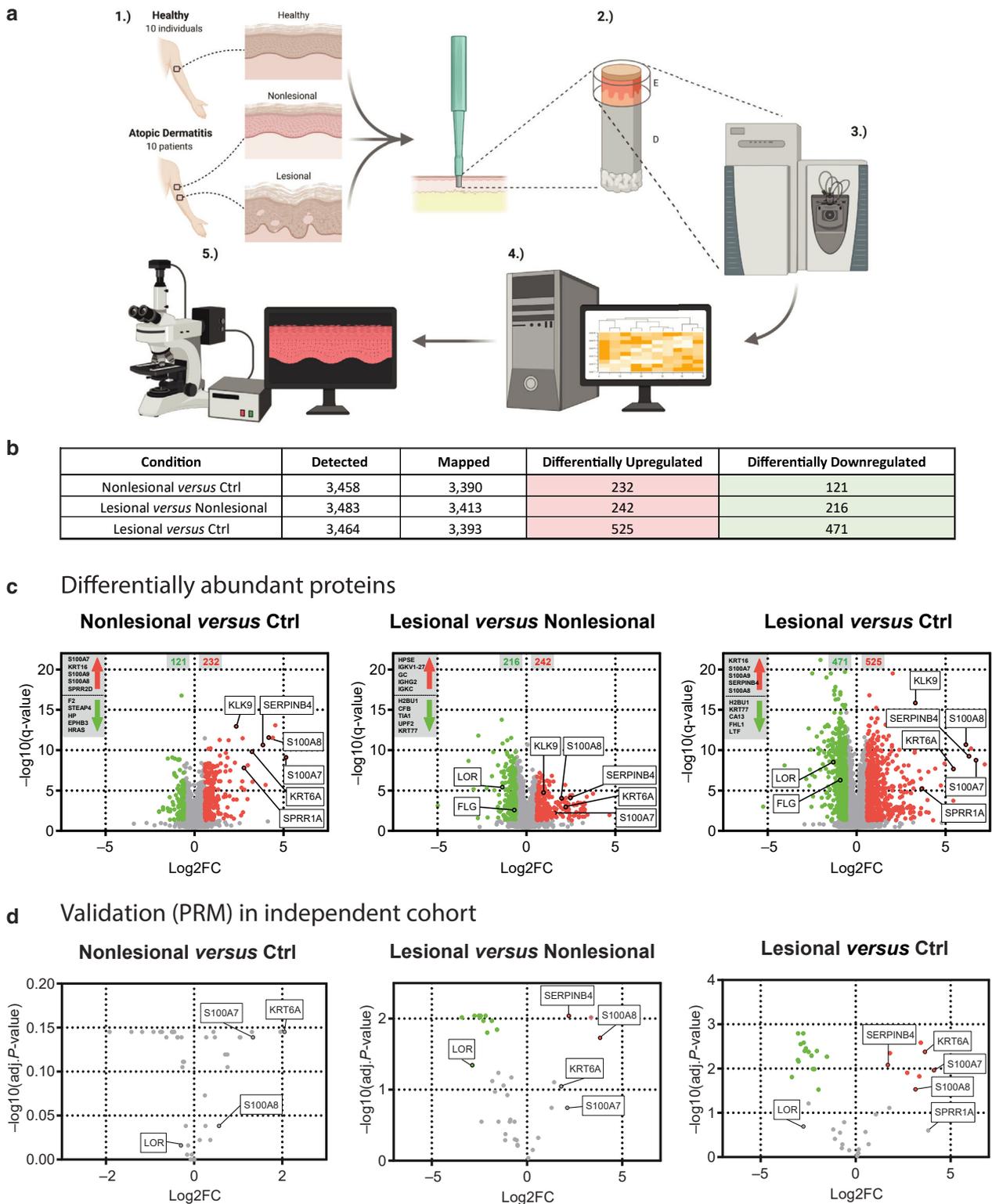
Figure 1. Quantitative proteomics of epidermis from patients with AD and healthy individuals and validation of selected hits. (**a**) Workflow of the proteomics experiment, including biopsy (n = 10 L, NL, and Ctrl samples), isolation of epidermis, label-free MS-based quantitative proteomics, and validation. (**b**) The numbers of proteins detected and mapped in all the three comparisons and the number of proteins with significantly differential abundances (Log2FC > 0.58 or < −0.58; FDR = 0.05) between conditions. (**c**) Volcano plots showing protein ratios between conditions. Proteins with significantly differential abundance (adj. q ≤ 0.05, Log2FC > 0.58 or < −0.58; FDR = 0.05) are shown in red (increased in abundance) or green (decreased in abundance). (**d**) Volcano plots showing the protein ratios between conditions, determined by PRM analysis in samples from an independent cohort. Significantly (adj. *P*-values [BH] are shown) differentially abundant proteins are shown. AD, atopic dermatitis; adj., adjusted; BH, Benjamini−Hochberg; Ctrl, control; FDR, false discovery rate; L, lesional; Log2FC, log$_2$ fold change; MS, mass spectrometry; NL, nonlesional; PRM, parallel reaction monitoring.

Table 1. Data from Patients and Healthy Volunteers Used for Proteomics (Patients and Healthy Volunteers Used for Large-Scale Quantitative Proteomics)

Patient Number	ID	Age	Sex	Location	SCORAD	FLG Status
AD 1	ZETH_01 NL/L	23	f	Upper arm left	52	WT
AD 2	ZETH_02 NL/L	38	f	Shoulder left	27	HE
AD 3	ZETH_03 NL/L	20	m	Thigh left	33	WT
AD 4	ZETH_04 NL/L	23	m	Upper arm right	44	HO/compound HE
AD 5	ZETH_05 NL/L	47	m	Lower back	41	WT
AD 6	ZETH_21 NL/L	63	m	Thigh left	65	HO/compound HE
AD 7	ZETH_22 NL/L	20	f	Arm right	45	HE
AD 8	ZETH_23 NL/L	20	f	Axillary right	37	HE
AD 9	ZETH_26 NL/L	54	m	Lower back	53	WT
AD 10	ZETH_27 NL/L	77	m	Upper arm left	46	WT
CTRL 1	ZETH_09	44	f	Back		WT
CTRL 2	ZETH_13	23	f	Upper arm left		HE
CTRL 3	ZETH_14	40	m	Lower back		WT
CTRL 4	ZETH_17	27	m	Upper arm right		WT
CTRL 5	ZETH_20	22	m	Thigh right		WT
CTRL 6	ZETH_24	26	f	Axillary right		WT
CTRL 7	ZETH_25	28	m	Thigh left		WT
CTRL 8	ZETH_28	28	m	Upper arm left		WT
CTRL 9	ZETH_29	50	m	Lower back		WT
CTRL 10	ZETH_30	24	f	Upper arm right		WT

Abbreviations: AD, atopic dermatitis; CTRL, control; f, female; HE, heterozygous; HO, homozygous; ID, identification; L, lesional; m, male; NL, nonlesional; SCORAD, SCORing Atopic Dermatitis; WT, wild-type.

defense (Goleva et al., 2020; He et al., 2020a; Morelli et al., 2021; Sakabe et al., 2014; Winget et al., 2016). Proteomics of skin organoids, using KCs with *FLG* knockdown, showed a reduced abundance of proteins involved in terminal differentiation and alterations in innate and adaptive immunity compared with that of Ctrl organoids (Elias et al., 2019). However, the proteome of the full epidermis of patients with AD in vivo has not been analyzed so far. In addition, it is unclear how the epidermal proteome of nonlesional (NL) AD skin differs from the proteome of healthy individuals.

In this study, we performed quantitative proteomics of the full epidermis from lesional and NL skin of adult patients with AD and healthy volunteers, which revealed a deficiency in the NRF2-mediated oxidative stress response as well as a reduced abundance of various mitochondrial proteins in AD skin.

RESULTS
Quantitative proteomics uncovers major molecular alterations in AD skin

To characterize the epidermal proteome of AD skin, we collected 5-mm punch biopsies from 10 healthy volunteers (Ctrl) and from the lesional and NL skin of 10 adult patients with chronic AD (Figure 1a and Tables 1 and 2). Epidermal lysates were subjected to data-independent acquisition label-free quantitative MS-based proteomics (Bachofner et al., 2017) (Figure 1a). We identified 3,516 protein groups with data completeness of ∼70% and library recovery >99%, of which 3,458 could be relatively quantified in samples from NL versus Ctrl skin, 3,483 could be relatively quantified in lesional versus NL skin, and 3.464 could be relatively quantified in lesional versus Ctrl skin (Figure 1b and Supplementary Table S1). The purity of the epidermis was reflected by the strong enrichment of epidermal proteins. The

abundance of proteins specifically expressed in basal KCs (e.g., integrins α6 and β4) excluded an epidermal split. A large number of proteins was significantly differentially abundant between Ctrl or NL versus lesional AD skin (Figure 1b and c). Interestingly, 232 proteins were already significantly higher in NL than in Ctrl skin, and 121 proteins were significantly lower in abundance. The top hits among

Table 2. Data from Patients and Healthy Volunteers Used for PRM Validation

Patient Number	ID	Age	Sex	Location	SCORAD	FLG Status
AD 11	ZETH_101 NL/L	49	m	Popliteal fossa left	44.5	HE
AD 12	ZETH_102 NL/L	23	f	Lower back left	32	WT
AD 13	ZETH_103 NL/L	49	m	Popliteal fossa left	63	WT
AD 14	ZETH_104 NL/L	51	m	Lower abdomen right	42	HE
AD 15	ZETH_105 NL/L	19	f	Elbow right	62	HE
CTRL 11	ZETH_106	23	f	Lower back left		WT
CTRL 12	ZETH_107	50	m	Popliteal fossa left		WT
CTRL 13	ZETH_108	44	m	Lower abdomen right		WT
CTRL 14	ZETH_109	49	m	Popliteal fossa left		WT
CTRL 15	ZETH_110	27	f	Flank right		WT

Abbreviations: AD, atopic dermatitis; CTRL, control; f, female; HE, heterozygous; HO, homozygous; ID, identification; L, lesional; m, male; NL, nonlesional; PRM, parallel reaction monitoring; SCORAD, SCORing Atopic Dermatitis; WT, wild-type.

the proteins that were more abundant in NL than in Ctrl skin include various proteins that reflect the impaired KC differentiation and epidermal barrier function (S100A7, keratin [K] 16) as well as proteinases and their inhibitors (Figure 1c, left panel, with the five top hits in the gray box). These results highlight that differentiation/barrier function abnormalities and low-grade inflammation are already present in NL skin.

The differences were even more pronounced in lesional skin, reflecting the phenotype progression from NL to lesional skin. This was also shown by the strong clustering of the lesional, NL, and Ctrl data by principal component analysis, whereas the results were independent of the body site (Supplementary Figure S1a).

Although the data clustered remarkably well among the analyzed patients, we validated the results with epidermal samples from five additional patients with AD and five healthy individuals (Tables 1 and 2) by targeted proteomics using parallel reaction monitoring-MS. We reliably comparatively quantified 39 proteins in lesional versus in NL skin, 43 in NL versus in Ctrl skin, and 44 in lesional versus in Ctrl skin. Because of lower sample sizes (n = 5), the results did not reach the same statistical power as in the discovery experiment, but a differential abundance of known critical disease markers as well as effect sizes were confirmed for all the three comparisons (Figure 1d and Supplementary Tables S1 and S2).

Decreased abundance of proteins involved in epidermal barrier function and high abundance of inflammatory mediators in AD epidermis

Various members of the S100 protein family were strongly increased in abundance in lesional skin, including S100A7 and S100A8, which are overexpressed in several inflammatory skin diseases (Eckert et al., 2004) (Figure 1c and Supplementary Table S1). Additional proteins that were significantly more abundant in lesional skin include proteinases and their inhibitors (e.g., KLK9 and SERPINB4) (Figure 1c and d), which contribute to barrier disruption in AD (Morizane, 2019; Sivaprasad et al., 2015), as well as K6A, K16, and K17, which are characteristic for activated interfollicular KCs (Supplementary Figure S1b and Supplementary Tables S1 and S3). K8, which is usually restricted to simple epithelia, was increased in abundance as well as K24, which is associated with KCs senescence (Min et al., 2017).

Among the proteins that were significantly less abundant in lesional skin were the cornified envelope proteins FLG and loricrin, which is consistent with the impaired epidermal barrier and abnormal KCs proliferation (Figure 1c and Supplementary Figure S1b). As expected, FLG levels were further decreased in the epidermis of patients with AD carrying heterozygous sequence variants for *FLG* and even more in patients with homozygous or compound heterozygous sequence variants, further confirming the validity of our proteomics data (Supplementary Figure S1c). Other cornified envelope proteins were increased in abundance, including some small proline-rich protein family members (Figure 1c and Supplementary Figure S1b). Further marker proteins for epidermal differentiation, including involucrin and transglutaminases (TGM1, TGM3, TGM5), were also dysregulated in the AD epidermis (Supplementary Figure S1b). The levels

of K6A or SPRR1B were not affected by *FLG* sequence variants (Supplementary Figure S1c and Supplementary Table S4).

A comparison of the proteomics data with published bulk RNA-sequencing data from AD epidermis isolated by laser capture microdissection (Esaki et al., 2015) showed that only 7.37% (±1.52%) of the differentially abundant proteins were also differentially regulated at the RNA level (Supplementary Table S5).

Reduced activity of the cytoprotective NRF2 pathway in AD epidermis

Pathway enrichment analysis revealed that proteins, which were already more abundant in NL than in Ctrl skin and even further increased in lesional skin, play a role in acute-phase response signaling or blood coagulation (Figure 2a and Supplementary Table S6). There was also a strongly increased abundance of complement proteins but only in the lesional skin (Supplementary Table S7). Overall, the pathways that were activated reflect the well-documented immunological alterations and inflammation in AD skin. By contrast, some of the pathways that showed reduced activation in AD skin had previously not been associated with this disease. In particular, proteins involved in xenobiotic metabolism or signaling through the NRF2 transcription factor showed lower abundance already in NL AD epidermis and particularly in lesional AD epidermis (Figure 2a). Because NRF2 is a key regulator of the cellular antioxidant defense system (Baird and Yamamoto, 2020; Sykiotis and Bohmann, 2010), downregulation of this pathway indicates a deficiency of KCs in the detoxification of xenobiotic compounds and of ROS. Concomitantly, pathways involved in the production of ROS or reactive nitrogen species were activated (Figure 2a and Supplementary Table S6). Several NRF2 targets were significantly less abundant in lesional epidermis than in NL epidermis, including glutathione reductase, GSTM2, and SOD3 (Figure 2b). Analysis of publicly available single-cell RNA-sequencing data (He et al., 2020b) revealed that major NRF2-target genes were expressed at lower levels in basal and suprabasal KCs of AD versus in Ctrl epidermis (Supplementary Figure S2a and Supplementary Table S8). In particular, the classical NRF2 target gene *NQO1*, which is mainly regulated by NRF2 (Dinkova-Kostova and Talalay, 2010), was strongly downregulated, whereas expression of the genes encoding the negative regulators of NRF2 activity, valosin-containing protein and BACH1, was mildly upregulated. Downregulation in AD skin was confirmed for *GSTM3* and *SOD3* when we analyzed bulk RNA-sequencing data from laser-capture−isolated epidermis or total skin of patients with AD (Esaki et al., 2015; Suárez-Fariñas et al., 2015), whereas information about other major NRF2 targets could not be obtained from these data. Together, these findings provide strong evidence for impaired activation of the NRF2 pathway in AD epidermis and may explain the previously described oxidative stress in AD skin (Bertino et al., 2020).

Because of the unexpected impairment of NRF2 activation, we focused further validation experiments on NRF2 targets or inhibitors. According to Ingenuity Pathway Analysis and literature search, 13 proteins, which had been described as general or cell type−specific NRF2 targets and which are
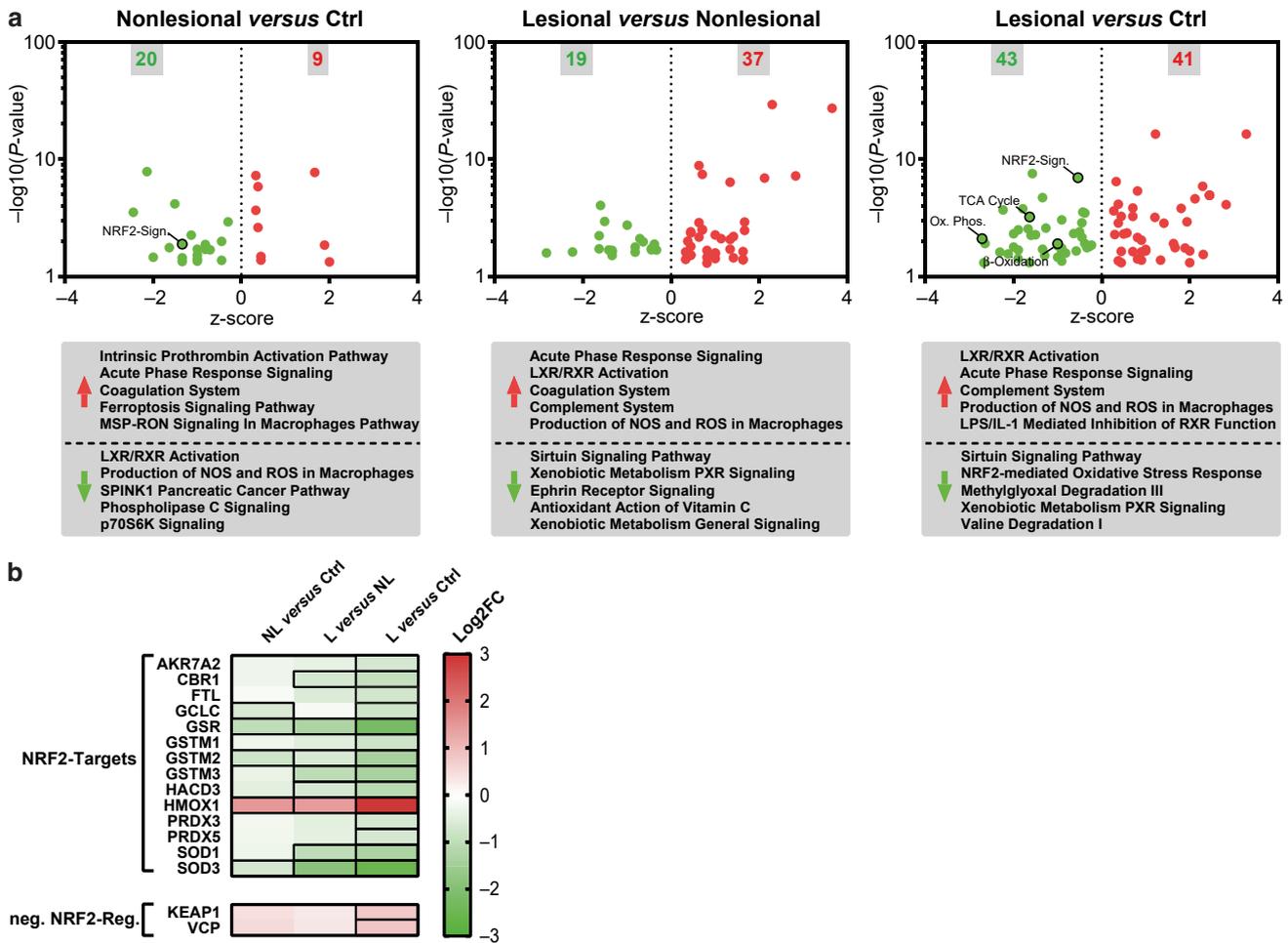
Figure 2. Reduced NRF2 pathway activation in AD skin. (**a**) Volcano plots showing the differentially regulated pathways in the epidermis of NL versus Ctrl, L versus NL, and L versus Ctrl skin. The top five pathways of proteins with increased or decreased abundance are shown below. (**b**) Heatmap showing reduced (green) or increased (red) abundance of previously described NRF2 targets and of the negative NRF2 regulators KEAP1 and VCP in the epidermis of NL versus Ctrl, L versus NL, and L versus Ctrl skin (see also Supplementary Table S9). Proteins with significantly differential abundance (q-value < 0.05; Log2FC ≤ 0.58 or > 0.58) are indicated with a black box. AD, atopic dermatitis; Ctrl, control; L, lesional; Log2FC, log₂ fold change; neg., negative; NL, nonlesional; VCP, valosin-containing protein;

involved in the cellular antioxidant defense and/or phase II detoxification, were significantly lower in abundance in lesional skin, and some of them were already reduced in NL skin (Figure 2b and Supplementary Table S9). The only NRF2 target that was more abundant in AD skin was HMOX1 (Figure 2b). *HMOX1* expression is also regulated by increased ROS levels through other ROS-sensitive transcription factors, for example, activator protein 1 (Keyse and Tyrrell, 1989; Medina et al., 2020). Therefore, the oxidative stress in AD epidermis is likely to activate these transcription factors, resulting in NRF2-independent *HMOX1* upregulation.

The levels of the NRF2 antagonist KEAP1 and of valosin-containing protein (Figure 2b), which is required for efficient proteasomal degradation of NRF2 (Tao et al., 2017), were increased in lesional epidermis, which provides a possible explanation for the reduced NRF2 activity. Notably, glutathione reductase was lower in abundance in 10 of 10 patients with AD in all the three comparisons, and KEAP1 protein levels were higher in NL than in Ctrl skin of 8 of 10 patients with AD, in lesional than in NL skin of 7 of

10 patients, and in lesional than in Ctrl skin of 10 of 10 patients (Supplementary Figure S2b and c). The regulation of glutathione reductase, SOD3, and KEAP1 was independent of the status of *FLG* sequence variation (Supplementary Figure S3a).

The reduced activation of NRF2 in AD skin was verified by staining the skin sections from independent patients with an antibody against Ser40 phosphorylated NRF2. This antibody was chosen because the weakening of the NRF2–KEAP1 interaction and subsequent nuclear accumulation of NRF2 require Ser40 phosphorylation (Bloom and Jaiswal, 2003) and because the levels of NRF2 in the nucleus are relevant for its function in transcriptional regulation (Baird and Yamamoto, 2020). We observed a reduction in the number of KCs with nuclear phosphorylated NRF2 in lesional skin (Figure 3a and b), which was already visible but less pronounced in NL skin (Supplementary Figure S3b). Reduced staining in acute and chronic AD lesions was also observed for NQO1, whereas BACH1, a transcriptional repressor that antagonizes NRF2 activity (Oyake et al., 1996), was
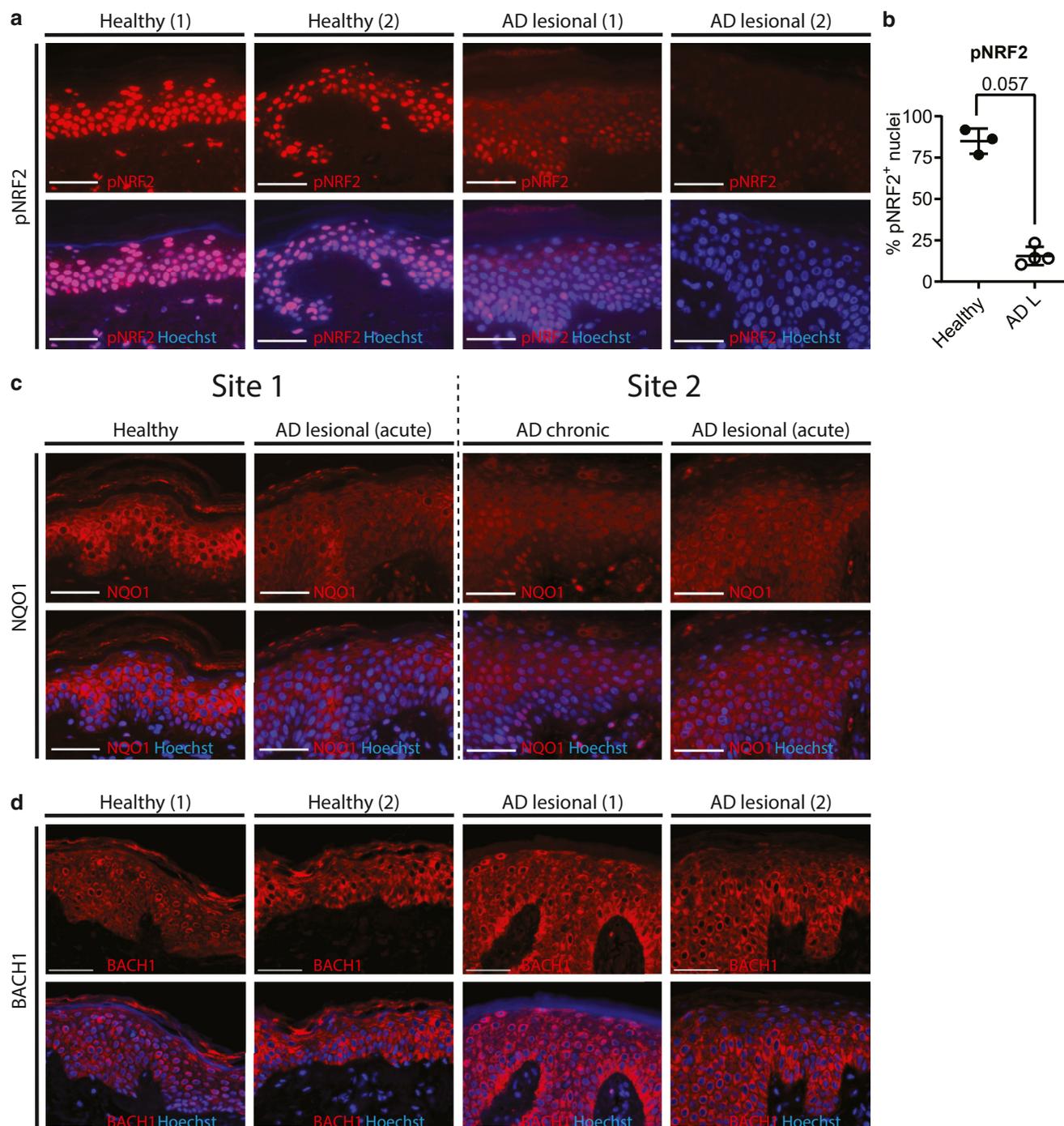
Figure 3. Reduced levels of pNRF2 and NQO1 but not of BACH1 in the epidermis of patients with AD. (**a**) Photomicrographs showing representative immunofluorescence staining of Ctrl and L skin for pNRF2 (red) and counterstaining of nuclei with Hoechst (blue). Bars = 50 μm. (**b**) Quantification of the percentage of pNRF2-positive nuclei per area of the epidermis. $P = 0.057$ (Mann–Whitney U test). Each dot represents one patient or a healthy volunteer. A total of 5–10 fields of view were counted per patient/volunteer. n = 3–4. (**c**, **d**) Photomicrographs showing a representative immunofluorescence staining of Ctrl and L skin (acute and chronic lesions as indicated) for (**c**) NQO1 (red) or (**d**) BACH1 (red) and counterstaining of nuclei with Hoechst (blue). n = 3 AD and 4 Ctrl samples each. Bars = 50 μm. AD, atopic dermatitis; Ctrl, control; L, lesional; pNRF2, phosphorylated NRF2.

expressed at similar levels in the epidermis of AD and Ctrl skin (Figure 3c and d).

Reduced abundance of mitochondrial proteins in AD epidermis
Another remarkable feature of lesional epidermis was the strongly reduced abundance of various mitochondrial proteins (Figures 2a and 4a and b and Supplementary Table S10). Many of them were also downregulated at the RNA level (He et al., 2020b). However, the reduction at the protein level was more robust (Supplementary Figure S4a).

Important examples of mitochondrial proteins that were less abundant in AD epidermis are the NRF2 targets PRDX3
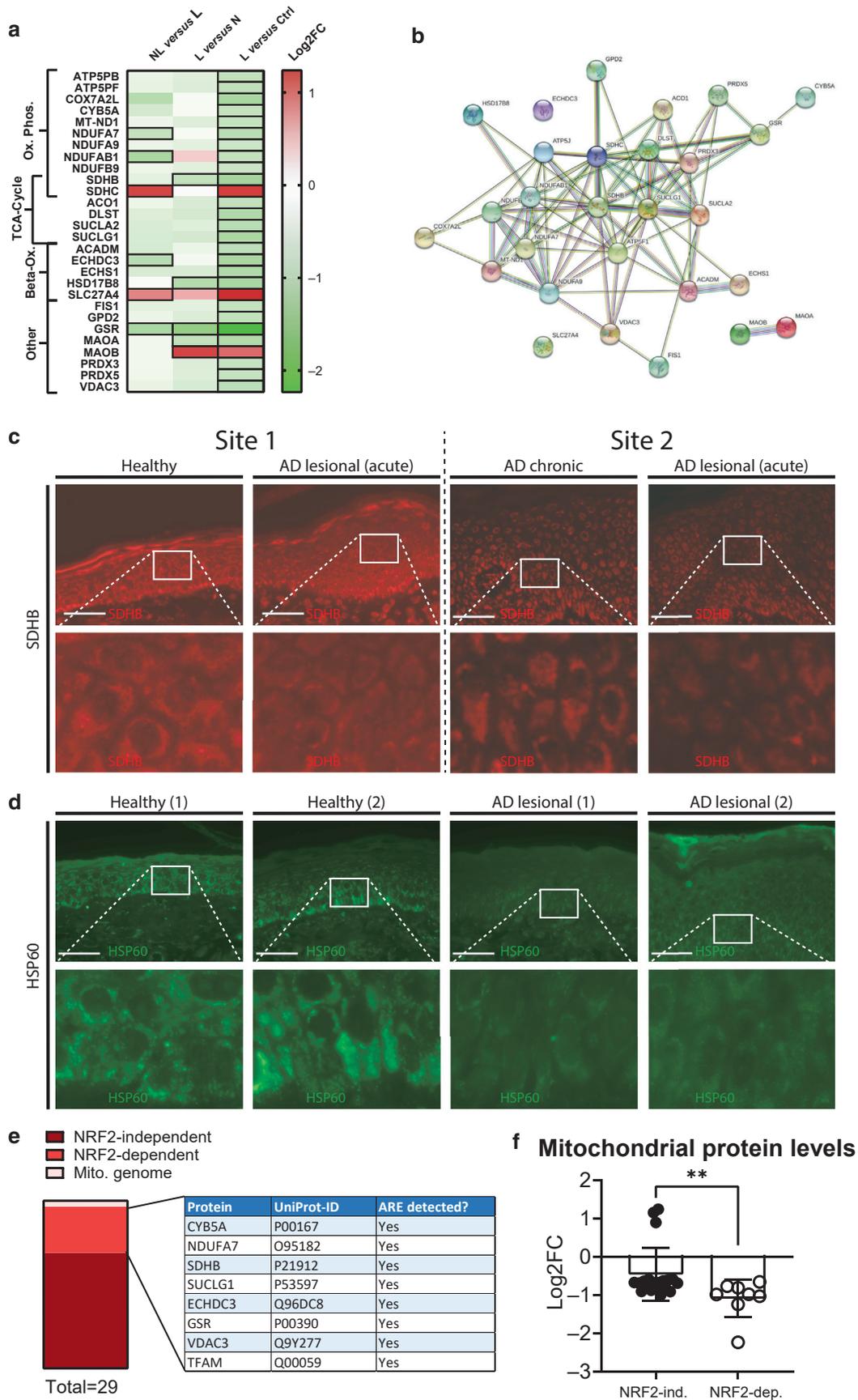
Figure 4. Reduced abundance of mitochondrial proteins in the epidermis of patients with AD. (**a**) Heatmap showing reduced (green) or increased (red) abundance of mitochondrial proteins in the epidermis of NL versus Ctrl, L versus NL, and L versus Ctrl skin (see Supplementary Table S10). Proteins with significantly differential abundance (q-value < 0.05; Log2FC ≤ 0.58 or > 0.58) are indicated with a box. (**b**) STRING protein interaction analysis of

and PRDX5, which are involved in ROS detoxification, as well as proteins involved in the tricarboxylic acid cycle, oxidative phosphorylation, or β-oxidation. These include, among others, SDHB and COX7A2L, which are components of the respiratory chain, as well as ECHDC3 and HSD17B8, which are involved in fatty acid metabolism. Their levels were independent of the status of *FLG* sequence variation (Supplementary Figure S4b).

The reduced abundance of SDHB in AD epidermis was confirmed by immunofluorescence staining of sections from independent patients (Figure 4c). Staining for the mitochondrial marker and housekeeping protein HSP60 was also strongly reduced in all tested samples of the lesional skin (Figure 4d).

NRF2 regulates a subset of mitochondrial proteins in human KCs

To determine whether the reduced NRF2 activation and the lower abundance of mitochondrial proteins are interlinked, we reanalyzed our published data obtained by chromatin immunoprecipitation and sequencing, which had been obtained with primary human KCs treated with the NRF2-activating compound sulforaphane or vehicle (Kurinna et al., 2021). Of the 29 differentially abundant mitochondrial proteins, eight showed binding of NRF2 in the regulatory regions of their genes (Figure 4e). Those eight proteins are encoded by the nuclear genome, and their abundance was particularly low in AD skin (Figure 4f).

To further determine the potential effect of NRF2 on mitochondrial proteins in KCs, we performed small interfering RNA–mediated knockdown of *NRF2* in human primary KCs. After 72 hours, expression of *NRF2,* expression of two classical NRF2 target genes (*NQO1* and *GCLC*), and expression of the putative NRF2 target *CYB5A* (Kurinna et al., 2021) were significantly downregulated with both small interfering RNAs (Figure 5a). Among other mitochondrial proteins that were reduced in abundance in AD epidermis, only the mRNA levels of *COX7A2L* were mildly downregulated with both small interfering RNAs (Figure 5a). Western blot analysis confirmed the downregulation of phosphorylated NRF2 and NQO1 by both NRF2 small interfering RNAs, whereas expression levels of HSP60 and SDHB were not affected (Figure 5b). This finding suggests that *NRF2* knockdown does not directly affect the levels of most mitochondrial proteins. This is supported by the lack of obvious differences in Mitotracker staining between immortalized human HaCaT KCs with or without *NRF2* knockdown (Figure 5c). As expected, *NRF2* knockdown mildly increased the levels of total intracellular ROS under homeostatic conditions, whereas the levels of mitochondrial ROS and cellular adenosine triphosphate were mildly reduced (Figure 5d–f).

Together, these results show that NRF2 directly regulates a subset of mitochondrial proteins at the transcriptional level,

whereas the global downregulation of other mitochondrial proteins in AD epidermis likely involves indirect mechanisms, which may be related to chronic inflammation.

DISCUSSION

We present a comprehensive proteomics dataset of the full epidermis from lesional and NL AD skin and from the skin of healthy individuals. Using data-independent acquisition, we generated digital proteome maps, which can be queried for specific proteins using alternative peptide libraries or provide assays for targeted analyses of proteins in normal or diseased skin.

The surprisingly small overlap between differentially abundant mRNAs and proteins in AD versus in Ctrl epidermis points to a key relevance of post-transcriptional regulation of gene/protein expression in AD skin. However, it should be considered that various lowly abundant proteins could not be detected in our MS-based proteomics analysis owing to the high tissue complexity. Furthermore, RNAs/proteins that are differentially abundant in one dataset might be below the threshold limits of significance in the other and thus not included in the analysis, although their regulation still shows a similar trend. Therefore, our study nicely complements previous transcriptomics results.

An unexpected finding was the impaired NRF2 activity in AD epidermis. We chose this pathway for further analysis because of (i) its consistent downregulation in AD skin, (ii) the lack of previous data on NRF2 activity in this disease, and (iii) the possibility to activate NRF2 by well-characterized compounds (Hayes et al., 2010). The reduced abundance of NRF2-target proteins was already observed in the NL epidermis, suggesting that it is not the consequence of strong inflammation. Therefore, reduced NRF2 activation is obviously not sufficient to induce an AD phenotype. Rather, it is likely to promote oxidative stress and inflammation in response to a proinflammatory stimulus. Consistent with this assumption, *Nrf2*-knockout mice do not have obvious skin abnormalities under homeostatic conditions. However, knockout of *Nrf2* enhanced UV-induced KC apoptosis in mouse epidermis (Schäfer and Dütsch, 2010) and further delayed the wound healing process in mice with diabetes (Long et al., 2016). Most importantly, *Nrf2*-knockout mice showed increased numbers of neutrophils in the skin on induction of contact dermatitis, which was a consequence of oxidative stress and enhanced chemokine production (Helou et al., 2019). They were also more sensitive to radiation-induced dermatitis (Schmidlin et al., 2020). NRF2 is also a key regulator of the epidermal barrier, which activates a rescue pathway in loricrin-deficient mice. The combined loss of loricrin and NRF2 signaling in KCs caused perinatal death of mice because of an impaired epidermal barrier and consequent desiccation (Huebner et al., 2012; Ishitsuka and

mitochondrial proteins shown in **a** that were differentially abundant in the epidermis of L versus Ctrl skin. (**c**, **d**) Representative immunofluorescence staining of Ctrl and L skin (acute and chronic lesions as indicated) for (**c**) SDHB (red) or (**d**) HSP60 (green) (n = 4 each). The area indicated by the white rectangle is shown at higher magnification below. Bars = 50 μm. (**e**) Stacked bar chart showing mitochondrial proteins that are less abundant in AD epidermis. Eight of them (see Supplementary Table S10) showed NRF2 binding in their regulatory region in cultured keratinocytes (Kurinna et al., 2021). (**f**) Graph showing the Log2FC abundance differences between epidermis of AD and Ctrl skin for mitochondrial proteins with detected NRF2-binding sites in the regulatory region of their genes in cultured keratinocytes (n = 8) versus those without detectable NRF2-binding sites (n = 21) (Kurinna et al., 2021). **$P = 0.0039$ (Mann–Whitney *U* test). AD, atopic dermatitis; Ctrl, control; L, lesional; Log2FC, log$_2$ fold change; NL, nonlesional.
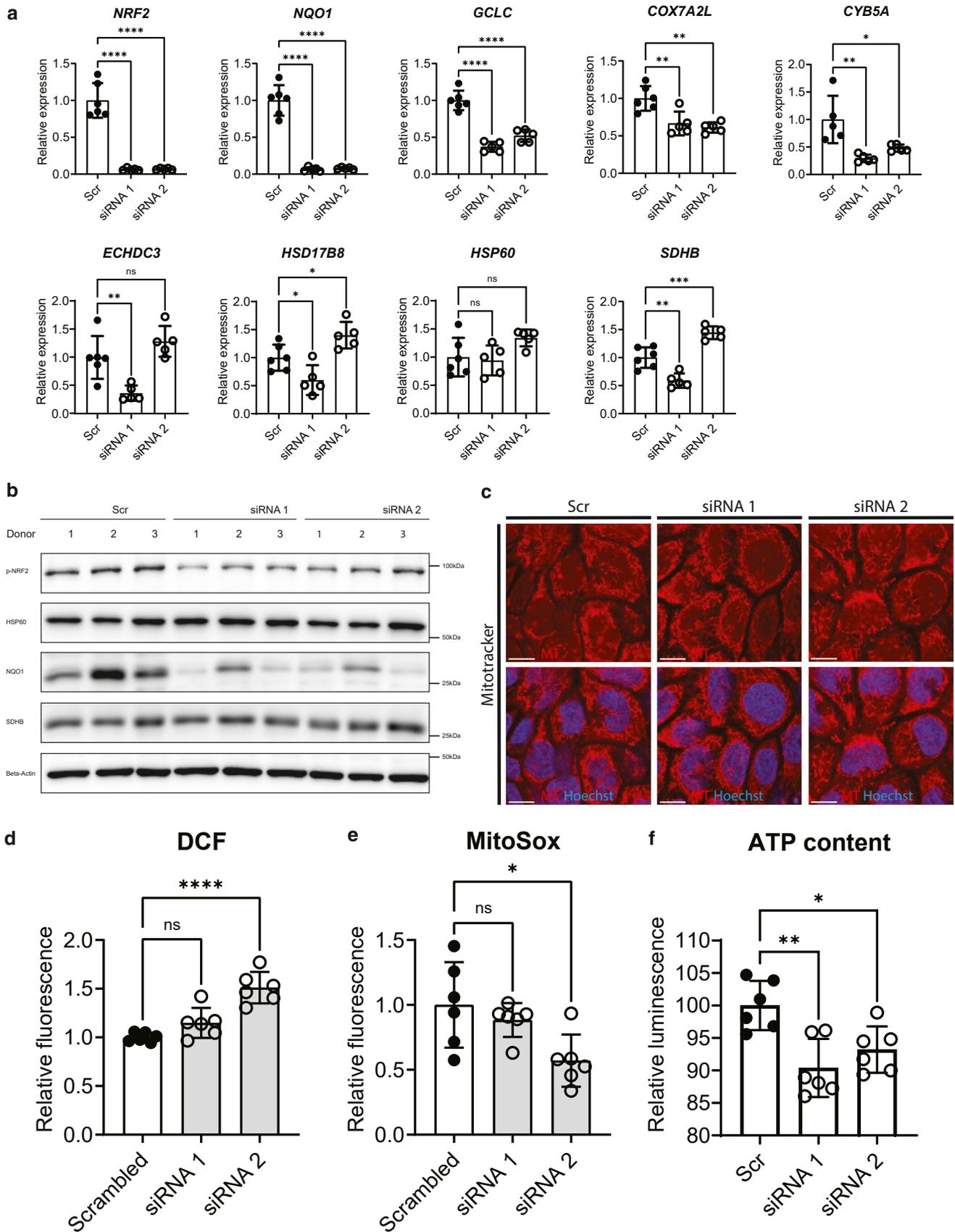
Figure 5. A subset of mitochondrial genes/proteins is directly regulated by NRF2. (**a**) qRT-PCR using RNA from primary human keratinocytes transfected with Scr or NRF2 siRNAs (siRNA1, siRNA2) for expression of *NRF2, NQO1, GCLC, CYB5A, COXA2L, HSD17B8, HSP60, ECHDC3,* and *SDHB*. (**b**) Western blot of human primary keratinocytes with or without *NRF2* knockdown for pNRF2, HSP60, NQO1, SDHB, and β-actin (loading control). (**c**) Representative photomicrographs of HaCaT keratinocytes with or without NRF2 knockdown stained with MT (red) and Hoechst (blue), analyzed by confocal microscopy.

Roop, 2021). However, overactivation of NRF2 in KCs of transgenic mice also resulted in a defective barrier. This was caused by corneocyte fragility as a result of an imbalance of different cornified envelope proteins (Schäfer et al., 2012). Together, these findings show that the amount and activity of NRF2 in KCs has to be tightly regulated to maintain an efficient barrier. The reduced NRF2 activation in AD skin may therefore contribute to the barrier deficiency and also enhance the susceptibility to skin inflammation.

Although we were not able to detect NRF2 by MS-based proteomics, the normal *NRF2* mRNA levels in AD epidermis (He et al., 2020b) show that activation rather than the expression of NRF2 is affected, possibly because of a higher abundance of NRF2 inhibitors. Therefore, NRF2-activating compounds appear promising for the treatment of AD as exemplified by their beneficial effects in experimentally induced AD in mice (Wu et al., 2019; Yoo et al., 2020). Furthermore, agonists of the aryl hydrocarbon receptor, which also activate NRF2, for example, coal tar and tapinarof, showed efficacy for AD in clinical trials (Furue, 2020; Peppers et al., 2019; van den Bogaard et al., 2013).

Another unexpected finding was the reduced abundance of various mitochondrial proteins in AD epidermis. This may result in part from a reduction in the number of mitochondria but also from reduced expression of specific mitochondrial proteins. It is also possible that the mitochondria are defective in AD epidermis, for example, as a consequence of long-term oxidative stress. This hypothesis is in line with the abnormal perinuclear clustering of mitochondria observed in AD skin (Huck et al., 2016). Defective mitochondria likely cause impairments in the tricarboxylic acid cycle, β-oxidation, and oxidative phosphorylation in AD, and the down-regulation of proteins involved in these pathways was indeed observed in our study. This may result in a switch from oxidative phosphorylation to glycolysis. In line with this hypothesis, reduced levels of β-oxidation metabolites and enhanced levels of lactate were detected in the serum of patients with AD (Ottas et al., 2017).

The impaired NRF2 activation and reduced abundance of mitochondrial proteins may be partially interlinked because NRF2 deficiency impacted cellular bioenergetics in murine neurons and fibroblasts by controlling substrate availability for mitochondrial respiration (Holmström et al., 2013) and affected the efficiency of mitochondrial fatty acid oxidation (Ludtmann et al., 2014). Consistent with these findings, mitochondrial ROS and cellular adenosine triphosphate levels were mildly reduced in *NRF2*-knockdown KCs (this study). Together, these results point to the role of NRF2 in mitochondrial respiration and energy production. We also showed that a subset of mitochondrial proteins that are less abundant in AD skin is encoded by direct *NRF2*-target genes. These genes are present in the nuclear genome, which is consistent with the nuclear localization of NRF2. Furthermore, nuclear respiratory factor 1, a key regulator of mitochondrial biogenesis, was shown to be controlled by NRF2,

and *Nrf2*-knockout mice failed to elevate nuclear respiratory factor 1 levels and mitochondrial biogenesis during *Staphylococcus aureus*−induced pneumonia (Athale et al., 2012). Although we were not able to detect nuclear respiratory factor 1 in our proteomics study, these findings point to the possible impairment of mitochondrial biogenesis on reduction of NRF2 activity. Together, the results presented in this study suggest that NRF2 activity regulates mitochondria at different levels, which is consistent with its previously shown activities in mitochondrial biogenesis, respiration, and quality control (Ryoo and Kwak, 2018). They also identify mitochondria as a possible pharmacological target in the treatment and/or prevention of AD.

MATERIALS AND METHODS
Patient selection
All patients were white Caucasians who had chronic disease without flares at the time of sampling. Biopsies were obtained from body sites with little sun exposure. Detailed information about the patients is provided in Tables 1 and 2. Skin from healthy volunteers was used as a Ctrl. Samples were obtained as part of an investigator-initiated clinical study to determine the molecular signatures of AD. Procedures were conducted according to the Declaration of Helsinki principles. Informed written consent was obtained from all participants under a protocol approved by the local ethics board at the University Hospital Schleswig-Holstein, Campus Kiel (Kiel, Germany) (reference number A100/12). Inclusion criteria for patients were a dermatologist-confirmed diagnosis of active AD according to standard criteria (Weidinger and Novak, 2016). Exclusion criteria were the presence of another chronic skin disease, previous or current systemic treatment with immune modulatory medication, or topical treatment within 1 week before the biopsy. Patients were screened for the four most common *FLG* sequence variants in the European population and categorized into either wild-type, heterozygous, or homozygous/compound heterozygous (Tables 1 and 2). Biopsies were analyzed by large-scale quantitative proteomics or targeted proteomics (Supplementary Materials and Methods).

Statistical analysis
Statistical analysis was performed using GraphPad Prism, version 8 (GraphPad Software, La Jolla, CA). Mean and SD are shown. Mann−Whitney U test was used for comparison between two groups. For comparison between three or more groups, one-way ANOVA test was used. $*P > 0.05$, $**P > 0.01$, $***P > 0.001$, and $****P > 0.0001$. For the data-independent acquisition proteomics data, differential protein abundances between sample groups were determined by unpaired Student's t-test and q-values generated using Storey's multiple testing correction method (Storey, 2002) implemented in Spectronaut. Statistical significance for parallel reaction monitoring data was determined by Student's t-test and Benjamini−Hochberg multiple testing correction (implemented in Skyline).

Data availability statement
The proteomics data are summarized in Supplementary Tables S1 and S2. Discovery proteomics data have been deposited to the ProteomeXchange Consortium (http://proteomecentral.

Bars = 10 μm. (**d**, **e**) Relative levels of (**c**) intracellular ROS or (**d**) mitochondrial superoxide in HaCaT cells transfected with Scr or NRF2 siRNAs. (**f**) Relative ATP levels in human primary keratinocytes transfected with Scr or NRF2 siRNAs. Bar graphs indicate mean ± SD. $*P < 0.05$, $**P < 0.01$, $***P < 0.001$, and $****P < 0.0001$ (one-way ANOVA). ATP, adenosine triphosphate; ns, not significant; MT, Mitotracker; pNRF2, phosphorylated NRF2; Scr, scrambled; siRNA, small interfering RNA.

ORCIDs
Michael Koch: http://orcid.org/0000-0003-2797-3227
Tobias Kockmann: http://orcid.org/0000-0002-1847-885X
Elke Rodriguez: http://orcid.org/0000-0003-3692-3950
Ulrike Wehkamp: http://orcid.org/0000-0002-7398-4261
Paul Hiebert: http://orcid.org/0000-0001-8179-4217
Maya Ben-Yehuda Greenwald: http://orcid.org/0000-0002-6089-0856
Dora Stölzl: http://orcid.org/0000-0002-7682-6373
Hans-Dietmar Beer: http://orcid.org/0000-0002-8085-713X
Erwin Tschachler: http://orcid.org/0000-0002-0248-1798
Stephan Weidinger: http://orcid.org/0000-0003-3944-252X
Sabine Werner: http://orcid.org/0000-0001-7397-8710
Ulrich auf dem Keller: http://orcid.org/0000-0002-3431-7415

Disclaimer
This publication reflects only the author's view, and the Joint Undertaking is not responsible for any use that may be made of the information it contains.

CONFLICT OF INTEREST
The authors state no conflict of interest.

AUTHOR CONTRIBUTIONS
Conceptualization: MK, SWei, SWer, UadK; Data Curation: TK, UadK; Formal Analysis: MK, TK, ET, UadK; Funding Acquisition: SWei, SWer, UadK; Investigation: MK, TK, ER, UW, PH, MBYG, DS, HDB, ET; Methodology: TK, UadK; Resources: ET, SWei; Supervision: SWei, SWer, UadK; Visualization: MK, UadK; Writing - Original Draft Preparation: MK, SW, UadK; Writing - Review and Editing: MK, TK, ER, UW, PH, MBYG, DS, HDB, ET, SWei, SWer, UadK.

SUPPLEMENTARY MATERIAL
Supplementary material is linked to the online version of the paper at www.jidonline.org, and at https://doi.org/10.1016/j.jid.2022.08.048

REFERENCES
Athale J, Ulrich A, MacGarvey NC, Bartz RR, Welty-Wolf KE, Suliman HB, et al. Nrf2 promotes alveolar mitochondrial biogenesis and resolution of lung injury in Staphylococcus aureus pneumonia in mice. Free Radic Biol Med 2012;53:1584−94.

Bachofner M, Speicher T, Bogorad RL, Muzumdar S, Derrer CP, Hürlimann F, et al. Large-scale quantitative proteomics identifies the ubiquitin ligase Nedd4-1 as an essential regulator of liver regeneration. Dev Cell 2017;42:616−25.e8.

Baird L, Yamamoto M. The molecular mechanisms regulating the KEAP1-NRF2 pathway. Mol Cell Biol 2020;40. e00099-20.

Bertino L, Guarneri F, Cannavò SP, Casciaro M, Pioggia G, Gangemi S. Oxidative stress and atopic dermatitis. Antioxidants (Basel) 2020;9:196.

Bloom DA, Jaiswal AK. Phosphorylation of Nrf2 at Ser40 by protein kinase C in response to antioxidants leads to the release of Nrf2 from INrf2, but is not required for Nrf2 stabilization/accumulation in the nucleus and transcriptional activation of antioxidant response element-mediated NAD(P)H:

quinone oxidoreductase-1 gene expression. J Biol Chem 2003;278:44675−82.

Brown SJ, Elias MS, Bradley M. Genetics in atopic dermatitis: historical perspective and future prospects. Acta Derm Venereol 2020;100:adv00163.

Deckers IA, McLean S, Linssen S, Mommers M, van Schayck CP, Sheikh A. Investigating international time trends in the incidence and prevalence of atopic eczema 1990-2010: a systematic review of epidemiological studies. PLoS One 2012;7:e39803.

Dinkova-Kostova AT, Talalay P. NAD(P)H:quinone acceptor oxidoreductase 1 (NQO1), a multifunctional antioxidant enzyme and exceptionally versatile cytoprotector. Arch Biochem Biophys 2010;501:116−23.

Eckert RL, Broome AM, Ruse M, Robinson N, Ryan D, Lee K. S100 proteins in the epidermis. J Invest Dermatol 2004;123:23−33.

Elias MS, Wright SC, Nicholson WV, Morrison KD, Prescott AR, Ten Have S, et al. Functional and proteomic analysis of a full thickness filaggrin-deficient skin organoid model. Wellcome Open Res 2019;4:134.

Esaki H, Ewald DA, Ungar B, Rozenblit M, Zheng X, Xu H, et al. Identification of novel immune and barrier genes in atopic dermatitis by means of laser capture microdissection. J Allergy Clin Immunol 2015;135:153−63.

Furue M. Regulation of filaggrin, loricrin, and involucrin by IL-4, IL-13, IL-17A, IL-22, AHR, and NRF2: pathogenic implications in atopic dermatitis. Int J Mol Sci 2020;21:5382.

Goleva E, Calatroni A, LeBeau P, Berdyshev E, Taylor P, Kreimer S, et al. Skin tape proteomics identifies pathways associated with transepidermal water loss and allergen polysensitization in atopic dermatitis. J Allergy Clin Immunol 2020;146:1367−78.

Guttman-Yassky E, Lowes MA, Fuentes-Duculan J, Whynot J, Novitskaya I, Cardinale I, et al. Major differences in inflammatory dendritic cells and their products distinguish atopic dermatitis from psoriasis. J Allergy Clin Immunol 2007;119:1210−7.

Hayes JD, McMahon M, Chowdhry S, Dinkova-Kostova AT. Cancer chemo-prevention mechanisms mediated through the Keap1-Nrf2 pathway. Anti-oxid Redox Signal 2010;13:1713−48.

He H, Olesen CM, Pavel AB, Clausen ML, Wu J, Estrada Y, et al. Tape-Strip proteomic profiling of atopic dermatitis on dupilumab identifies minimally invasive biomarkers. Front Immunol 2020a;11:1768.

He H, Suryawanshi H, Morozov P, Gay-Mimbrera J, Del Duca E, Kim HJ, et al. Single-cell transcriptome analysis of human skin identifies novel fibroblast subpopulation and enrichment of immune subsets in atopic dermatitis. J Allergy Clin Immunol 2020b;145:1615−28.

Helou DG, Noël B, Gaudin F, Groux H, El Ali Z, Pallardy M, et al. Cutting edge: Nrf2 regulates neutrophil recruitment and accumulation in skin during contact hypersensitivity. J Immunol 2019;202:2189−94.

Holmström KM, Baird L, Zhang Y, Hargreaves I, Chalasani A, Land JM, et al. Nrf2 impacts cellular bioenergetics by controlling substrate availability for mitochondrial respiration. Biol Open 2013;2:761−70.

Hönzke S, Wallmeyer L, Ostrowski A, Radbruch M, Mundhenk L, Schäfer-Korting M, et al. Influence of Th2 cytokines on the cornified envelope, tight junction proteins, and ß-defensins in filaggrin-deficient skin equivalents. J Invest Dermatol 2016;136:631−9.

Huck V, Gorzelanny C, Thomas K, Getova V, Niemeyer V, Zens K, et al. From morphology to biochemical state - intravital multiphoton fluorescence lifetime imaging of inflamed human skin. Sci Rep 2016;6:22789.

Huebner AJ, Dai D, Morasso M, Schmidt EE, Schäfer M, Werner S, et al. Amniotic fluid activates the nrf2/keap1 pathway to repair an epidermal barrier defect in utero. Dev Cell 2012;23:1238−46.

Ishitsuka Y, Roop DR. The epidermis: redox governor of health and diseases. Antioxidants (Basel) 2021;11:47.

Keyse SM, Tyrrell RM. Heme oxygenase is the major 32-kDa stress protein induced in human skin fibroblasts by UVA radiation, hydrogen peroxide, and sodium arsenite. Proc Natl Acad Sci USA 1989;86:99−103.

Kurinna S, Seltmann K, Bachmann AL, Schwendimann A, Thiagarajan L, Hennig P, et al. Interaction of the NRF2 and p63 transcription factors promotes keratinocyte proliferation in the epidermis. Nucleic Acids Res 2021;49:3748−63.

Leung DYM, Calatroni A, Zaramela LS, LeBeau PK, Dyjack N, Brar K, et al. The nonlesional skin surface distinguishes atopic dermatitis with food allergy as a unique endotype. Sci Transl Med 2019;11:eaav2685.

Long M, Rojo de la Vega M, Wen Q, Bharara M, Jiang T, Zhang R, et al. An essential role of NRF2 in diabetic wound healing. Diabetes 2016;65: 780−93.

Lou H, Lu J, Choi EB, Oh MH, Jeong M, Barmettler S, et al. Expression of IL-22 in the skin causes Th2-biased immunity, epidermal barrier dysfunction, and pruritus via stimulating epithelial Th2 cytokines and the GRP pathway. J Immunol 2017;198:2543−55.

Ludtmann MH, Angelova PR, Zhang Y, Abramov AY, Dinkova-Kostova AT. Nrf2 affects the efficiency of mitochondrial fatty acid oxidation. Biochem J 2014;457:415−24.

Medina MV, Sapochnik D, Garcia Solá M, Coso O. Regulation of the expression of heme Oxygenase-1: signal transduction, gene promoter activation, and beyond. Antioxid Redox Signal 2020;32:1033−44.

Min M, Chen XB, Wang P, Landeck L, Chen JQ, Li W, et al. Role of keratin 24 in human epidermal keratinocytes. PLoS One 2017;12:e0174626.

Mitamura Y, Nunomura S, Nanri Y, Ogawa M, Yoshihara T, Masuoka M, et al. The IL-13/periostin/IL-24 pathway causes epidermal barrier dysfunction in allergic skin inflammation. Allergy 2018;73:1881−91.

Morelli P, Gaspari M, Gabriele C, Dastoli S, Bennardo L, Pavel AB, et al. Proteomic analysis from skin swabs reveals a new set of proteins identifying skin impairment in atopic dermatitis. Exp Dermatol 2021;30:811−9.

Morizane S. The role of kallikrein-related peptidases in atopic dermatitis. Acta Med Okayama 2019;73:1−6.

Nomura I, Gao B, Boguniewicz M, Darst MA, Travers JB, Leung DY. Distinct patterns of gene expression in the skin lesions of atopic dermatitis and psoriasis: a gene microarray analysis. J Allergy Clin Immunol 2003;112: 1195−202.

Ottas A, Fishman D, Okas TL, Püssa T, Toomik P, Märtson A, et al. Blood serum metabolome of atopic dermatitis: altered energy cycle and the markers of systemic inflammation. PLoS One 2017;12:e0188580.

Oyake T, Itoh K, Motohashi H, Hayashi N, Hoshino H, Nishizawa M, et al. Bach proteins belong to a novel family of BTB-basic leucine zipper transcription factors that interact with MafK and regulate transcription through the NF-E2 site. Mol Cell Biol 1996;16:6083−95.

Peppers J, Paller AS, Maeda-Chubachi T, Wu S, Robbins K, Gallagher K, et al. A phase 2, randomized dose-finding study of tapinarof (GSK2894512 cream) for the treatment of atopic dermatitis. J Am Acad Dermatol 2019;80:89−98.e3.

Perez-Riverol Y, Csordas A, Bai J, Bernal-Llinares M, Hewapathirana S, Kundu DJ, et al. The PRIDE database and related tools and resources in 2019: improving support for quantification data. Nucleic Acids Res 2019;47:D442−50.

Ryoo IG, Kwak MK. Regulatory crosstalk between the oxidative stress-related transcription factor Nfe2l2/Nrf2 and mitochondria. Toxicol Appl Pharmacol 2018;359:24−33.

Sakabe J, Kamiya K, Yamaguchi H, Ikeya S, Suzuki T, Aoshima M, et al. Proteome analysis of stratum corneum from atopic dermatitis patients by hybrid quadrupole-Orbitrap mass spectrometer. J Allergy Clin Immunol 2014;134. 957−60.e8.

Schäfer M, Dütsch S, auf dem Keller U, Navid F, Schwarz A, Johnson DA, et al. Nrf2 establishes a glutathione-mediated gradient of UVB cytoprotection in the epidermis. Genes Dev 2010;24:1045−58.

Schäfer M, Farwanah H, Willrodt AH, Huebner AJ, Sandhoff K, Roop D, et al. Nrf2 links epidermal barrier function with antioxidant defense. EMBO Mol Med 2012;4:364−79.

Schmidlin CJ, Rojo de la Vega M, Perer J, Zhang DD, Wondrak GT. Activation of NRF2 by topical apocarotenoid treatment mitigates radiation-induced dermatitis. Redox Biol 2020;37:101714.

Sivaprasad U, Kinker KG, Ericksen MB, Lindsey M, Gibson AM, Bass SA, et al. SERPINB3/B4 contributes to early inflammation and barrier dysfunction in an experimental murine model of atopic dermatitis. J Invest Dermatol 2015;135:160−9.

Storey JD. A direct approach to false discovery rates. J R Stat Soc B 2002;64: 479−98.

Suárez-Fariñas M, Ungar B, Correa da Rosa J, Ewald DA, Rozenblit M, Gonzalez J, et al. RNA sequencing atopic dermatitis transcriptome profiling provides insights into novel disease mechanisms with potential therapeutic implications. J Allergy Clin Immunol 2015;135: 1218−27.

Sykiotis GP, Bohmann D. Stress-activated cap'n'collar transcription factors in aging and human disease. Sci Signal 2010;3:re3.

Tao S, Liu P, Luo G, Rojo de la Vega M, Chen H, Wu T, et al. p97 negatively regulates NRF2 by extracting ubiquitylated NRF2 from the KEAP1-CUL3 E3 complex. Mol Cell Biol 2017;37. e00660-16.

Tsoi LC, Rodriguez E, Degenhardt F, Baurecht H, Wehkamp U, Volks N, et al. Atopic dermatitis is an IL-13-dominant disease with greater molecular heterogeneity compared to psoriasis. J Invest Dermatol 2019;139:1480−9.

van den Bogaard EH, Bergboer JG, Vonk-Bergers M, van Vlijmen-Willems IM, Hato SV, van der Valk PG, et al. Coal tar induces AHR-dependent skin barrier repair in atopic dermatitis. J Clin Invest 2013;123:917−27.

Weidinger S, Beck LA, Bieber T, Kabashima K, Irvine AD. Atopic dermatitis. Nat Rev Dis Primers 2018;4:1.

Weidinger S, Novak N. Atopic dermatitis. Lancet 2016;387:1109−22.

Winget JM, Finlay D, Mills KJ, Huggins T, Bascom C, Isfort RJ, et al. Quantitative proteomic analysis of stratum corneum dysfunction in adult chronic atopic dermatitis. J Invest Dermatol 2016;136:1732−5.

Wu W, Peng G, Yang F, Zhang Y, Mu Z, Han X. Sulforaphane has a therapeutic effect in an atopic dermatitis murine model and activates the Nrf2/HO-1 axis. Mol Med Rep 2019;20:1761−71.

Yoo OK, Choi WJ, Keum YS. Cardamonin inhibits oxazolone-induced atopic dermatitis by the induction of NRF2 and the inhibition of Th2 cytokine production. Antioxidants (Basel) 2020;9:834.

SUPPLEMENTARY MATERIALS AND METHODS

Patient samples used for proteomics experiments

Patients with AD used for large-scale quantitative proteomics (n = 10) included four female and six male individuals with a median age of 31 years. Healthy volunteers (n = 10) included four female and six male individuals with a median age of 28 years. For parallel reaction monitoring (PRM) validation, we used five additional patients with AD, including two female and three male individuals with a median age of 49 years. Healthy volunteers (n = 5) included two female and three male individuals with a median age of 44 years (Table 1).

For validation of results by immunofluorescence, we used additional patients with chronic or acute AD and additional healthy individuals.

Sample processing

A total of 5 mm skin punch biopsies were obtained under local anesthesia from lesional skin of patients with chronic AD. Nonlesional skin was taken from an adjacent area at least 5 cm away from the active lesion. Biopsies were incubated for 1 minute in 60 °C PBS under swirling and cooled down for 1 minute in 4 °C PBS, allowing separation of epidermis and dermis without the use of enzymatic digestion. The epidermis was peeled off from the dermis using forceps and snap frozen in liquid nitrogen. For pressure-cycling technology, 2 mg of epidermal tissue was placed into pressure-cycling technology MicroTubes (catalog number: MT-96, Pressure BioSciences, Easton, MA). After adding 30 μl of freshly prepared lysis buffer (8 M urea, 100 mM ammonium bicarbonate, 1x complete protease inhibitors, EDTA-free), tubes were sealed using a pressure-cycling technology microPestle (C/N: MTWS-MP96-B, Pressure BioSciences). Pressure-assisted protein extraction and tandem digestion were performed as originally described (Guo et al., 2015) with the exception that Lys-C was used at 1:50, and trypsin was used at 1:40 w/w enzyme to substrate ratio. The resulting C18-cleaned peptides were diluted to 0.3 A280 U/ml using 3% acetonitrile/0.1% formic acid and mixed with iRT (stock keeping unit: Ki-3002, Biognosys, Schlieren, Switzerland) at a ratio of 1/20 (v/v). iRT peptides were used as standard in data-independent acquisition (DIA) experiments for indexed retention time normalization and significantly improved identification and quantitation (Bruderer et al., 2016).

DIA proteomics

Peptide samples were analyzed in DIA mode on a hybrid quadrupole-orbitrap mass spectrometer (Q Exactive HF, Thermo Fisher Scientific, Waltham, MA) equipped with a Digital PicoView source (New Objective, Woburn, MA) and operated in line with a nano ultraperformance liquid chromatography system (nanoACQUITY, Waters, Milford, MA). For each sample, 2 μl of purified peptide mixture were trapped on a nanoEase M/Z Symmetry C18 trap column (5 μm, 180 μm × 20 mm, Waters) and separated on a nanoEase M/Z HSS T3 C18 Column (100 å, 1.8 μm, 75 × 150 mm, Waters) at a flow rate of 300 nl/min using a gradient from 1% solvent B (0.1% formic acid in acetonitrile, Romil, Cambridge, United Kingdom)/99% solvent A (0.1 % formic acid in water, Romil) to 35% solvent B/65% solvent A within 90 minutes. Mass spectra were recorded at a resolution of 30,000 (at 200 m/z) in profile mode using positive polarity.

Mass spectrometry (MS) 1 scans covering 350−1,500 m/z were acquired using an automatic gain control target of 3e6 and a maximum IT of 41 ms. Each MS1 scan was followed by 32 multiplexed fragment ion scans (MS2) tiling the m/z range of 350−1,500 in 25-Da windows. The maximum injection time per MS2 scan was selected automatically by the instrument software to assure acquisition at a fixed scan rate of 12 Hz. Accordingly, the instrument cycle time was around 2.4 seconds at a chromatographic peak width of 20−30 seconds. The automatic gain control target for MS2 scans was set to 3e6, and isolated precursors were fragmented using higher-energy collisional dissociation at a normalized collision energy of 28.

Data analysis of DIA proteomics experiments

Raw MS data were analyzed with Spectronaut 14.10.201222.47784 (Biognosys) (Bruderer et al., 2015) using a hybrid spectral library compiled from recorded DIA runs and shotgun MS from pooled lesional, NL, and control samples searched against the Biognosys human Uniprot-Reference database uniprot_sprot_2020-01-01_HUMAN (20,367 entries) with default parameters. For analysis, default BGS Factory Settings were applied, quantitative data were exported from Post Analysis and Volcano plots, and principal component analysis was generated in GraphPad Prism, versions 8 and 9, respectively (GraphPad Software, La Jolla, CA).

PRM validation

PRM measurements were performed on a Q Exactive HF (Thermo Fisher Scientific) instrument equipped with a Digital PicoView source (New Objective) and operated in line with a nano ultraperformance liquid chromatography system (ACQUITY UPLC M-CLASS, Waters). Peptides were trapped on an M-CLASS Symmetry C18 trap column (5 μm, 180 μm × 20 mm, Waters) and separated on an M-CLASS HSS T3 C18 Column (100 å, 1.8 μm, 75 × 250 mm, Waters) at a flow rate of 300 nl/min using a gradient from 5% solvent B (0.1% formic acid in acetonitrile, Romil)/95% solvent A (0.1% formic acid in water, Romil) to 35% solvent B/65% solvent A within 60 minutes. The mass spectrometer was set to perform MS1 scans (150−2,000 m/z) with an automatic gain control target of 3e6, at a 120,000 resolution and with a maximum injection time of 200 ms followed by MS/MS acquisition in time-scheduled PRM mode with an automatic gain control target of 2e5, at a 30,000 resolution, an isolation window of 1.4 m/z, and a maximum injection time of 55 ms. Higher-energy collisional dissociation fragmentation was conducted at a normalized collision energy of 35%. The isolation lists for each performed assay are provided in Supplementary Table S2.

Data analysis for PRM proteomics experiments

Raw PRM data were analyzed using Skyline 3.7 (11371, MacCoss Lab, Seattle, WA) with a spectral library generated from the same shotgun MS analyses of a pooled sample as for the DIA analysis and selecting the top five b or y ions (≥3 ranks of series). All peaks were manually inspected for correct detection and boundaries, and peak areas were determined by the software. The Skyline group comparison algorithm was employed to calculate the ratios between

conditions using median equalization for normalization, a protein confidence interval of 95%, and Tukey's Median Polish as the summary method.

Immunofluorescence staining

Skin samples were stored in PAXgene tissue stabilizer reagent for 1–7 days at room temperature and embedded in paraffin. Sections (7 μm) were dewaxed and rehydrated using a xylene/ethanol gradient, followed by antigen retrieval using citrate buffer (100 mmol/l citric acid for NQO1 and BACH1, pH 6.0, and 10 mmol/l for all other antibodies) at 95 °C for 1 hour and three washes with PBS. Staining was performed using the following antibodies: mouse anti-HSP60 (number ab59457, Abcam, Cambridge, United Kingdom), rabbit anti–pSer40-NRF2 (number EP1809Y, Abcam), rabbit anti-NQO1 (number ab34173, Abcam), rabbit anti-BACH1 (number HPA034949, Sigma-Aldrich, St. Louis, MO), and rabbit anti-SDHB (number HPA002868, Sigma-Aldrich) and goat anti-mouse IgG–Cy2 (number 115 225 003, Jackson ImmunoResearch Laboratories, Westgrove, PA) and goat anti-rabbit IgG–Cy3 (number 111-165-003, Jackson ImmunoResearch Laboratories). Stained sections were analyzed using a Zeiss Imager.A1 microscope equipped with enhanced-contrast Plan-Neofluar objectives (40×/1.3 numeric aperture and 20×/0.5 numeric aperture) and photographed with an Axio-Cam MRm camera (all from Carl Zeiss, Oberkochen, Germany). ZEN blue software (version 2.6, Carl Zeiss) was used for data acquisition.

Small interfering RNA–mediated knockdown

Primary human keratinocytes were isolated from the foreskin of three independent donors without signs of skin disease as described previously (Sollberger et al., 2012). The human foreskin was obtained anonymously from healthy boys with written consent from the parents in the context of the University of Zurich biobank project approved by the local and cantonal Research Ethics Committees and according to the Declaration of Helsinki Principles. Knockdown of *NRF2* was performed by transfection of cells with two different small interfering RNAs (siRNAs) (GAGAAAGAAUUGCCUGUAA [deoxythymidine dinucleotide] for siRNA1 and CCUUAUU-CUCCUAGUGAAU [deoxythymidine dinucleotide] for siRNA2) using the INTERFERin siRNA transfection reagent (Polyplus, Illkirch-Graffenstaden, France). HaCaT cells (human immortalized keratinocytes [Boukamp et al., 1988]) were transfected with the same siRNAs using Lipofectamine RNAiMAX (Thermo Fisher Scientific). Scrambled siRNA was used as control (MISSION siRNA Universal Negative Control number1, number SIC001, Sigma-Aldrich). siRNA was added on days 1 and 3 after seeding. Cells were analyzed 24 hours after the second transfection.

RNA isolation and qRT-PCR

RNA isolation and qRT-PCR were performed as previously described (Hiebert et al., 2018, Rauschendorfer et al., 2021). Gene expression was normalized to *RPL27*. Primer sequences are listed in Supplementary Table S11.

Preparation of protein lysates and western blot

Keratinocytes were lysed in lysis buffer containing 50 mM Tris-hydrogen chloride, pH 8.0, 1% NP-40, and 150 mM sodium chloride and analyzed by western blot (Rauschendorfer et al., 2021) using the following primary antibodies: mouse anti-HSP60 (number ab59457, Abcam), rabbit antiphosphorylated Ser40 NRF2 (number EP1809Y, Abcam), rabbit anti-NQO1 (number ab34173, Abcam), rabbit anti-SDHB (number HPA002868, Sigma-Aldrich), mouse anti−β-actin (number A5441, Sigma-Aldrich), goat anti-mouse or anti-rabbit IgG, and horseradish peroxidase conjugate (number W402B or number W401B, respectively, Promega, Madison, WI).

Determination of cellular adenosine triphosphate levels

Adenosine triphosphate levels were measured using the CellTiter-Glo 2.0 Cell Viability Assay (number G9241, Promega) according to the manufacturer's instructions. Luminescence was recorded using the Cytation 3 Imaging Reader (BioTek, Winooski, VT) and analyzed using Gen5 All-In-One Microplate Reader Software (version 2.07, BioTek).

Determination of intracellular and mitochondrial ROS levels

Total cellular ROS were analyzed using H2DCFDA (D399, Thermo Fisher Scientific) as previously described (Hiebert et al., 2018). Mitochondrial ROS were analyzed using MitoSOX Red (Invitrogen, Waltham, MA) according to the manufacturer's instructions. Fluorescence was measured using a GloMax Microplate Reader (Promega).

Mitotracker staining of keratinocytes

HaCaT cells were stained with MitoTracker Orange CMTMRos (number M7510, Thermo Fisher Scientific) diluted 1:1,000 in a complete medium for 45 minutes at 37 °C) and costained with Hoechst 33342 (Sigma-Aldrich) diluted in PBS with 1% BSA for 30 minutes at room temperature. Confocal imaging was performed using a Leica TCS SP8 microscope equipped with a 40× 1.1 numerical aperture Water HC PL IRAPO objective. Laser power was kept constant throughout each experiment, as were photomultiplier tube voltage and gain. Leica SP8 LAS X software, version 3.5.5, was used to control the instrument and for image acquisition.

Pathway analysis

Proteomics datasets were analyzed using Ingenuity Pathway Analysis software (version 60467501, Qiagen, Hilden, Germany). Proteins with a q-value < 0.05 and a $\log_2$ fold change ≤ 0.58 or > 0.58 were included for analysis.

Image analysis

Immunofluorescence stainings were analyzed using ImageJ software (version 1.53e, National Institutes of Health, Bethesda, MD). To quantify the staining for phosphorylated NRF2, 10 images per stained section were acquired, and the number of phosphorylated NRF2^{+} nuclei in the epidermis was counted using the built-in cell counter tool and normalized to the total number of epidermal nuclei.

SUPPLEMENTARY REFERENCES

Boukamp P, Petrussevska RT, Breitkreutz D, Hornung J, Markham A, Fusenig NE. Normal keratinization in a spontaneously immortalized aneuploid human keratinocyte cell line. J Cell Biol 1988;106:761−71.

Bruderer R, Bernhardt OM, Gandhi T, Miladinović SM, Cheng LY, Messner S, et al. Extending the limits of quantitative proteome profiling with data-independent acquisition and application to acetaminophen-treated three-dimensional liver microtissues. Mol Cell Proteomics 2015;14:1400−10.

Bruderer R, Bernhardt OM, Gandhi T, Reiter L. High-precision iRT prediction in the targeted analysis of data-independent acquisition and its impact on identification and quantitation. Proteomics 2016;16:2246−56.

Guo T, Kouvonen P, Koh CC, Gillet LC, Wolski WE, Röst HL, et al. Rapid mass spectrometric conversion of tissue biopsy samples into permanent quantitative digital proteome maps. Nat Med 2015;21:407−13.

He H, Suryawanshi H, Morozov P, Gay-Mimbrera J, Del Duca E, Kim HJ, et al. Single-cell transcriptome analysis of human skin identifies novel fibroblast subpopulation and enrichment of immune subsets in atopic dermatitis. J Allergy Clin Immunol 2020;145:1615−28.

Hiebert P, Wietecha MS, Cangkrama M, Haertel E, Mavrogonatou E, Stumpe M, et al. Nrf2-mediated fibroblast reprogramming drives cellular senescence by targeting the matrisome. Dev Cell 2018;46. 145−61.e10.

Rauschendorfer T, Gurri S, Heggli I, Maddaluno L, Meyer M, Inglés-Prieto Á, et al. Acute and chronic effects of a light-activated FGF receptor in keratinocytes in vitro and in mice. Life Sci Alliance 2021;4:e202101100.

Sollberger G, Strittmatter GE, Kistowska M, French LE, Beer HD. Caspase-4 is required for activation of inflammasomes. J Immunol 2012;188: 1992−2000.
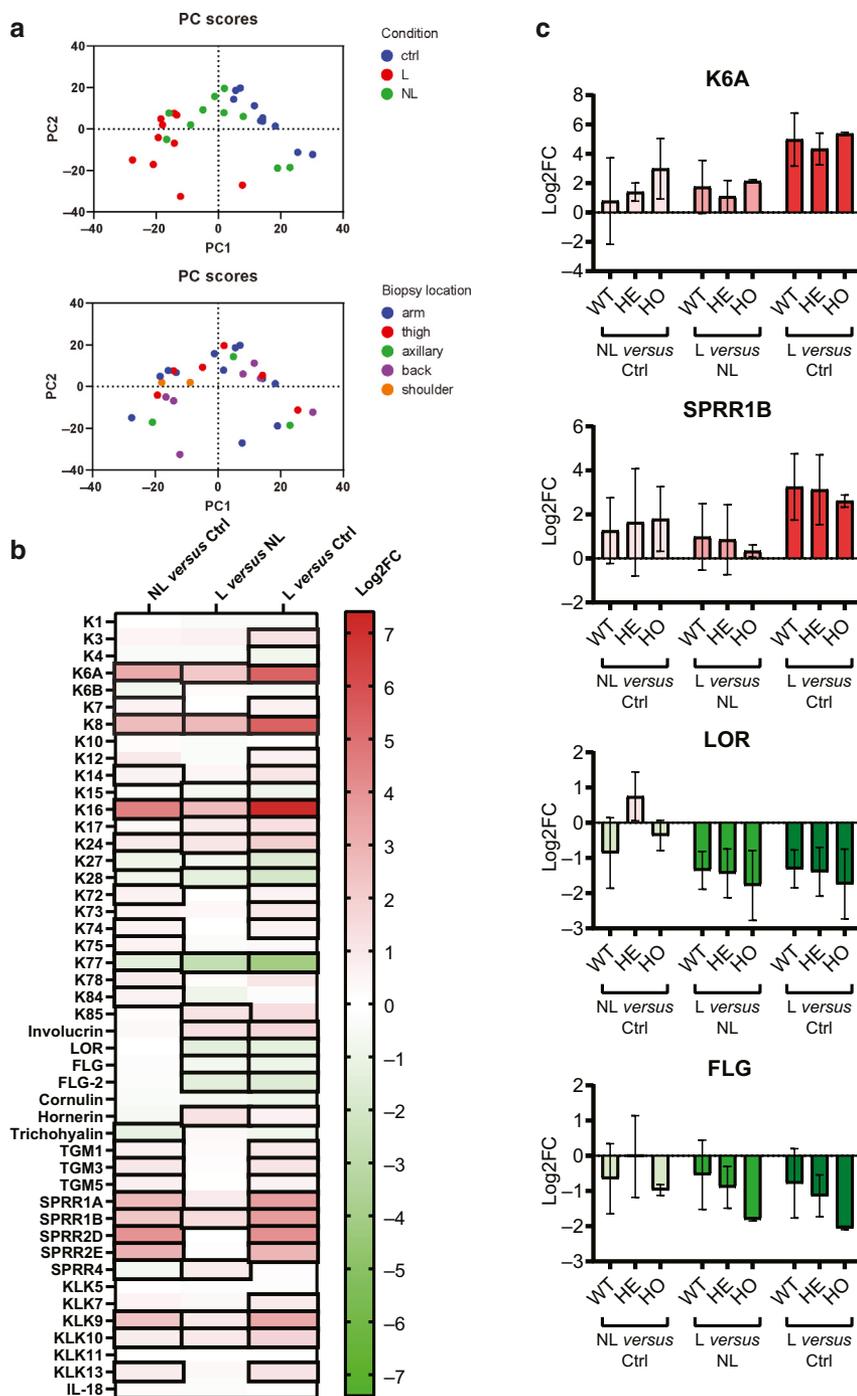
Supplementary Figure S1. Impaired keratinocyte differentiation and epidermal stratification in AD skin. (**a**) PCA score plot on the effect of conditions (Ctrl, NL, and L) shows a clear separation on the basis of the abundances of a total of 997 proteins as variables (top). PCA score plot on the effect of biopsy location (arm, thigh, axillary, back, and shoulder) shows no separation (bottom). (**b**) Heatmap showing reduced (green) or increased (red) abundance of proteins involved in keratinocyte differentiation/epidermal stratification in the epidermis of NL versus Ctrl, L versus NL, and L versus Ctrl skin. Proteins with significantly differential abundance (q-value < 0.05 and Log2FC ≤ 0.58 or > 0.58) are indicated with a black box. (**c**) Bar graphs showing increased or reduced abundance of the differentiation markers K6A, SPRR1B, LOR, and FLG in the epidermis of patients with AD with wild-type alleles for *FLG* (WT), HE *FLG* mutations, and HO/ compound HE mutations for *FLG*. Bars indicate mean ± SD. AD, atopic dermatitis; Ctrl, control; HE, heterozygous; HO, homozygous; K6A, keratin 6A; L, lesional; Log2FC, log$_2$ fold change; LOR, loricrin; NL, nonlesional; PCA, principal component analysis; WT, wild-type.
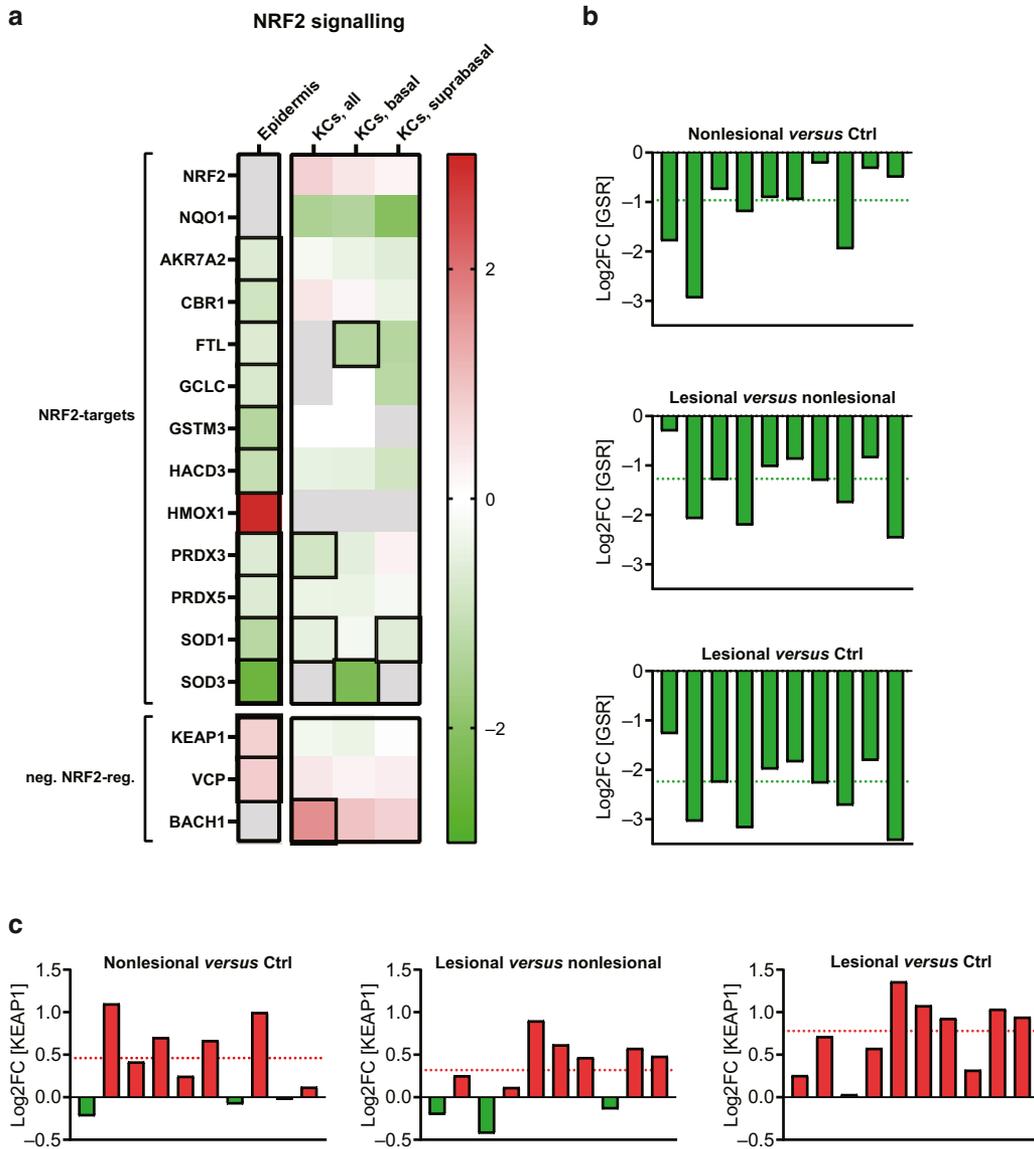
Supplementary Figure S2. NRF2-target genes are consistently downregulated at the RNA and protein level in AD epidermis, independent of the status of *FLG* sequence variation. (**a**) Heatmap showing reduced (green) or increased (red) abundance of proteins involved in NRF2 signaling in the epidermis of L versus Ctrl skin (left column) compared with the expression levels in basal, suprabasal, and total keratinocytes on the basis of published scRNA-seq data of L and Ctrl skin (He et al., 2020) (see also Supplementary Table S8). Proteins with significantly differential abundance (q-value < 0.05 and Log2FC ≤ 0.58 or > 0.58) are indicated with a black box. Proteins/genes that were not detected are indicated in gray. (**b**) Bar graphs showing reduced abundance (green) of GSR in the epidermis of NL vs Ctrl, L vs NL, and L vs Ctrl skin of individual patients. (**c**) Bar graphs showing increased (red) or reduced abundance (green) of KEAP1 in the epidermis of NL vs Ctrl, L vs NL, and L vs Ctrl skin of individual patients. AD, atopic dermatitis; Ctrl, control; L, lesional; Log2FC, log₂ fold change; neg., negative; NL, nonlesional; scRNA-seq, single-cell RNA sequencing.
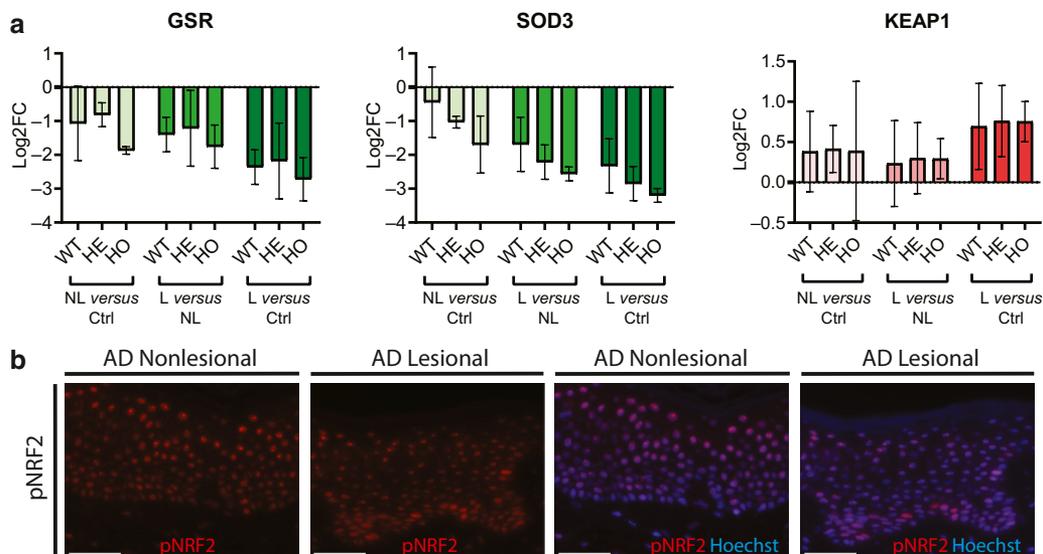
Supplementary Figure S3. Impaired NRF2 activation is independent of the status of *FLG* sequence variation and already detectable in non-lesional skin. (**a**) Bar graphs showing increased or reduced abundance of GSR, SOD3, and KEAP1 in the epidermis of patients with AD with WT alleles for *FLG*, HE sequence variants for *FLG,* and HO/compound HE sequence variants for *FLG*. Bars indicate mean ± SD. (**b**) Photomicrographs showing the representative immunofluorescence stainings of NL and L skin for pNRF2 (red) and counterstaining of nuclei with Hoechst (blue). Bars = 50 μm. AD, atopic dermatitis; GSR, glutathione reductase; HE, heterozygous; HO, homozygous; L, lesional; NL, nonlesional; pNRF2, phosphorylated NRF2; WT, wild-type.

Supplementary Figure S4. Mitochondrial proteins are downregulated at the RNA and protein level in AD epidermis, independent of the status of *FLG* sequence variation. (**a**) Heatmap showing reduced (green) or increased (red) abundance of mitochondrial proteins in the epidermis of L versus Ctrl skin (left column) compared with expression levels in basal, suprabasal, and total keratinocytes on the basis of published scRNA-seq data of L and Ctrl skin (He et al., 2020) (see also Supplementary Table S8). Proteins with significantly differential abundance (q-value < 0.05 and Log2FC $\leq$ 0.58 or > 0.58) are indicated with a black box. Proteins/genes that were not detected are indicated in gray. (**b**) Bar graphs showing increased or reduced abundance of the mitochondrial proteins SDHB, ECHDC3, and HSD17B8 in the epidermis of patients with AD with WT alleles for *FLG*, HE sequence variants for *FLG*, and HO/compound HE sequence variants for *FLG*. Bars indicate mean ± SD. AD, atopic dermatitis; Ctrl, control; HE, heterozygous; HO, homozygous; KC, keratinocyte; L, lesional; Log2FC, log$_2$ fold change; NL, nonlesional; scRNA-seq, single-cell RNA sequencing; WT, wild-type.
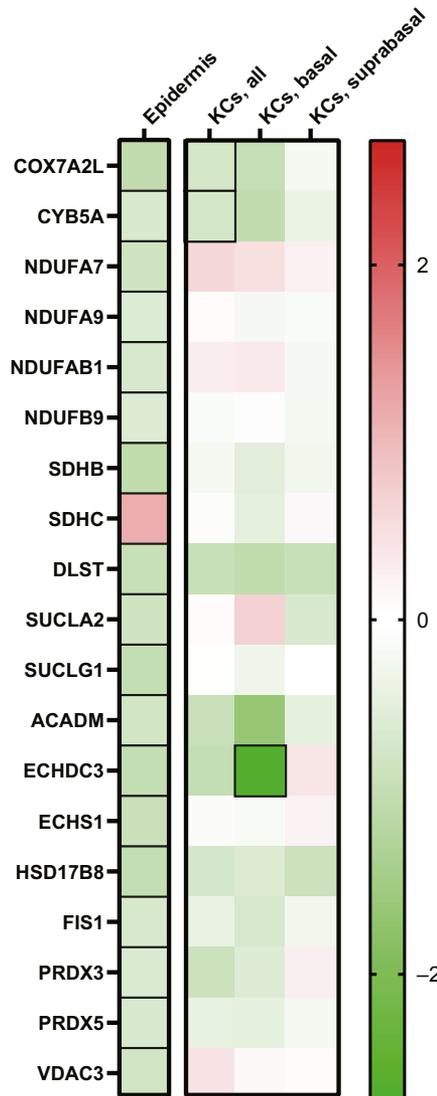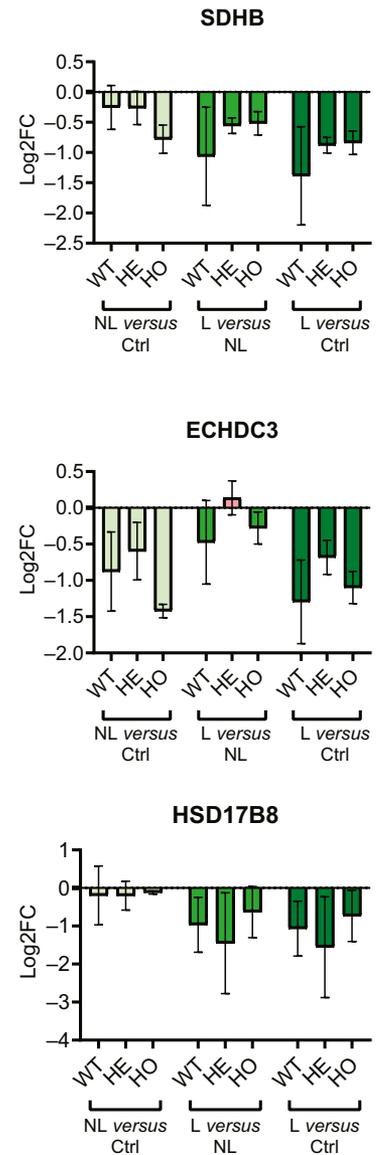
Supplementary Table S11. Primer Sequences Used in this Study

Gene	Forward Primer Sequence	Reverse Primer Sequence
COX7A2L	CACCAACTAAACTGACCTCCG	GGGCACACCATCAGCTTTCT
CYB5A	CACCACAAGGTGTACGATTTGA	CATCTGTAGAGTGCCCGACAT
ECHDC3	CTGGACGGCATAAGGAACATC	GACTTTCAGATCGTTGCTGTCA
GCLC	GGAAGGAAGGTGTGTTTCCTGG	ACTCCCTCATCCATCTGGCAA
HSD17B8	AGTAGCATCGTAGGAAAGGTGG	TGAGGTCCCTGTGATGTATCC
HSP60	ATGCTTCGGTTACCCACAGTC	AGCCCGAGTGAGATGAGGAG
NQO1	GTGATATTCCAGTTCCCCCTGC	AAGCACTGCCTTCTTACTCCGG
NRF2	AGGTTGCCCACATTCCCAAA	AATGTCTGCGCCAAAAGCTG
RPL27	TCA CCTAATGCCCACAAGGTA	CCACTTGTTCTTGCCTGTCTT
SDHB	CACTCTAGCTTGCACCCGAA	CGTAGAGCCCGTCCAGTTTC